8-5-2011

Characteristics of the Hydrogen Electrode in High Temperature Steam Electrolysis Process

Chao Jin

Chenghao Yang

Fanglin Chen
University of South Carolina - Columbia, chenfa@cec.sc.edu

Publication Info

Published in *Journal of The Electrochemical Society*, Volume 158, Issue 10, 2011, pages B1217-B1228.

Publisher's Version: http://dx.doi.org/10.1149/1.3615992
Jin, C., Yang, C., & Chen, F. (5 August 2011). Characteristics of the Hydrogen Electrode in High Temperature Steam Electrolysis Process. Journal of The Electrochemical Society, 158 (10), B1217 – B1228. http://dx.doi.org/10.1149/1.3615992

Journal of The Electrochemical Society, **158** (10) B1217-B1223 (2011)
0013-4651/2011/158(10)/B1217/7/$28.00 © The Electrochemical Society

Characteristics of the Hydrogen Electrode in High Temperature Steam Electrolysis Process

Chao Jin, Chenghao Yang,[*] and Fanglin Chen[,z]**

Department of Mechanical Engineering, University of South Carolina, Columbia, South Carolina 29208, USA

YSZ-electrolyte supported solid oxide electrolyzer cells (SOECs) using LSM-YSZ oxygen electrode but with three types of hydrogen electrode, Ni–SDC, Ni–YSZ and LSCM–YSZ have been fabricated and characterized under different steam contents in the feeding gas at 850°C. Electrochemical impedance spectra results show that cell resistances increase with the increase in steam concentrations under both open circuit voltage and electrolysis conditions, suggesting that electrolysis reaction becomes more difficult in high steam content. Pt reference electrode was applied to evaluate the contributions of the hydrogen electrode and oxygen electrode in the electrolysis process. Electrochemical impedance spectra and over potential of both electrodes were measured under the same testing conditions. Experimental results show that steam contents mainly affect the behavior of the hydrogen electrode but have little influence on the oxygen electrode. Further, contribution from the hydrogen electrode is dominant in the electrolysis process for Ni–based SOECs, but this contribution decreases for LSCM–based SOECs.
 [DOI: 10.1149/1.3615992]

Manuscript submitted April 8, 2011; revised manuscript received June 28, 2011. Published August 5, 2011.

In recently years, there has been an increasing interest in production of hydrogen as a secondary energy carrier.[1,2] Currently, hydrogen is primarily produced from steam reforming of methane.[2–4] However, methane reforming is not a sustainable process for large–scale hydrogen production from a long–term perspective since such a fossil fuel conversion process consumes nonrenewable resources and emits green house gases to the environment. An alternative method to produce hydrogen is via the electrolysis of water. Solid oxide electrolyzer cells (SOECs) are under developing and have gained much attention to generate hydrogen from electricity because water electrolysis at elevated temperature is advantageous for both thermodynamic and kinetic reasons.[5–7] Moreover, electricity and heat generated from the nuclear power systems and renewable energy sources, as well as waste heat from high temperature industrial processes can be utilized for electrolysis in SOECs.[8]

In principle, SOEC is essentially a reverse process of a solid oxide fuel cell (SOFC). Consequently, SOEC technology can be built on the SOFC technology which has made significant progress in recent years.[9–11] It has been well established that oxygen reduction reaction occurring in the oxygen electrode (cathode) is more sluggish and consequently the limiting factor for achieving high performances in SOFCs.[12–17] Significant efforts have accordingly been focused on the effects of the oxygen electrode in the electrolysis process but different conclusions exist in the reports for SOECs. Eguchi[10] found that a combination of LSM oxygen electrode and Ni–yttria stabilized zirconia (YSZ) hydrogen electrode performed better as an SOFC than as an SOEC, while LSC oxygen electrode combined with platinum hydrogen electrode showed lower polarization losses as an SOEC than as an SOFC. Jacobsen[18] reported that there was a significantly nonlinear behavior for Pt/YSZ oxygen electrode under cathodic *vs* anodic polarization, revealing that the Pt/YSZ electrode was considerably more active for oxygen ion oxidation than for oxygen reduction. O'Brien and co–workers,[7] however, observed very little differences in area specific resistance values between the fuel cell and electrolysis modes for an electrolyte–supported single cell with Ni/YSZ hydrogen electrode and LSM oxygen electrode. Wang and co-works[19] compared the performance of LSM, LSF, and LSCo for solid oxide electrolyzer anodes and found that LSM–YSZ electrode was unstable during the electrolysis, but LSF–YSZ and LSCo–YSZ electrodes exhibited nearly constant performance during both the SOEC and SOFC operations. Through a modeling study, Meng and co-workers[20] have found that the hydrogen electrode is vulnerable to high concentration overpotential and limiting current density in the SOEC mode while the oxygen electrode is vulnerable to high concentration overpotential and limiting current density in the SOFC mode. The above inconsistent observations may be due to the different operating conditions. However, there have been very few reports available to systematically characterize the hydrogen and oxygen electrode in high temperature steam electrolysis process.

In this work, the electrochemical properties, especially impedance spectra of YSZ electrolyte–supported SOECs with different hydrogen electrode (Ni–SDC, Ni–YSZ and LSCM–YSZ, respectively) but with the same oxygen electrode (LSM–YSZ) have been fabricated and characterized in the steam electrolysis process. Further, the cell electrochemical performances attributed to the hydrogen electrode and oxygen electrode have been separated via a three–electrode method to further study the contributions from the different electrodes in the steam electrolysis process.

Experimental

In this study, $La_{0.8}Sr_{0.2}MnO_{3-\delta}$ (LSM) powder and 8% mol yttria stabilized zirconia (YSZ) pellet (20 mm diameter and 0.3 mm thickness) were purchased from Fuel Cell Materials, USA. NiO was purchased from JT Baker, USA. YSZ (TZ–8Y) powder was purchased from TOSOH Corporation, Japan. $La_{0.75}Sr_{0.25}Cr_{0.5}Mn_{0.5}O_3$ (LSCM) and $Sm_{0.2}Ce_{0.8}O_{1.9}$ (SDC) powders were prepared through a sol–gel method.[21]

As shown in Table I, three types of cells were prepared and characterized. LSM/LSM–YSZ was selected as the oxygen electrode. Ni-SDC, Ni-YSZ and LSCM–YSZ were selected as the hydrogen electrode. Figure 1 shows the schematic diagram of the three–electrode method used in the study. NiO–YSZ and NiO–SDC hydrogen electrodes were prepared by mixing NiO and YSZ or SDC powders with a suitable amount of binder (ethyl cellulose and α–terpineol), followed by screen–printing on one side of YSZ pellet, and then sintered at 1400°C for 4 h. LSCM–YSZ hydrogen electrode was screen–printed on one side of YSZ pellet, followed by sintering at 1250°C for 3 h. The thickness of the hydrogen electrode is ~40 μm. For LSM/LSM–YSZ oxygen electrode, LSM–YSZ composite ink and pure LSM ink were symmetrically screen–printed on the other side of the YSZ pellet, opposite to the hydrogen electrode, and then sintered at 1200°C for 2 h. The thickness of the oxygen electrode is ~25 μm. The effective areas for both hydrogen and oxygen electrodes were 0.5 cm^2. Pt meshes were attached on the surface of each electrode as current collector. Pt reference electrode was deposited on the YSZ pellet of the oxygen electrode side, 3.9 mm away from the LSM–YSZ oxygen electrode. Both Pt meshes and Pt reference electrode were fired at 1000°C for 1 h. Pt lead wires were used to connect the electrodes to the electrochemical testing equipment. The button cells were sealed to one end of an alumina tube

* Electrochemical Society Student Member.
** Electrochemical Society Active Member.
z E-mail: chenfa@cec.sc.edu

Table I. Cell compositions and fabrication conditions.

	Hydrogen electrode (wt %)	Sintering	Oxygen electrode	Sintering
Cell–1	NiO-SDC (60:40)	1400°C 4 h	LSM/LSM–YSZ	1200°C 2 h
Cell–2	NiO-YSZ (60:40)	1400°C 4 h	LSM/LSM–YSZ	1200°C 2 h
Cell–3	LSCM-YSZ (60:40)	1250°C 3 h	LSM/LSM–YSZ	1200°C 2 h

with a ceramic paste (Aremco–552 high temperature ceramic adhesive paste).

The experimental setup for the steam electrolysis measurements was illustrated in Fig. 1 and the testing procedure was described in detail in our previous publications.[22–24] H_2 was selected as carrier gas to maintain the reducing environment in the hydrogen electrode. Open circuit voltages (OCVs) of the three types of cells with different steam content were summarized in Table II. These values were similar to those calculated using the Nernst equation. This demonstrates that the sealing used in the testing system is good and that there is no leaking between the hydrogen electrode and the oxygen electrode. The absolute humidity (AH, the vol % of humidity in the total gas volume) was used to represent steam concentrations in the electrolysis process. Electrochemical performances of the SOEC cells were studied using a conventional two–electrode method through a multi–channel VersaSTAT (Princeton Applied Research). Electrochemical impedance spectra (EIS) under both OCV and electrolysis conditions were performed over the frequency range of 100 kHz to 0.1 Hz. A reference electrode, as described by Jeremy,[25] was used in EIS and electrode overpotential tests in order to separate the contributions from the hydrogen and oxygen electrode under both OCV and electrolysis conditions.

Results and Discussion

Evaluation of cells with Ni–based hydrogen electrode.—The most commonly studied hydrogen electrode material for SOECs is Ni–based cermet. Voltage–current density relationship of cell–1 has been recorded using the two–electrode method for a series of steam concentrations (20, 40, and 60 vol % AH, respectively) under both the SOEC and SOFC modes at 850°C, as shown in Fig. 2. In the SOEC mode, negative current densities indicate power consumption to split water to produce hydrogen and oxygen. Cell potential values at zero current density correspond to the open circuit voltage (*OCV*). The cell *OCV* is influenced by the steam/hydrogen ratio, and deceases when the ratio increases, as expected from the Nernst Eq. (1)

$$E = E^0 + \frac{RT}{2F}\ln\left(\frac{p_{H_2}p_{O_2}^{1/2}}{p_{H_2O}}\right) \quad (1)$$

where E^0 is the standard electrode potential, R is the universal gas constant, T is the absolute temperature (K), F is the Faraday constant, and P_{H_2}, P_{O_2}, and P_{H_2O} denote the partial pressure of hydrogen, oxygen and steam, respectively. As shown in Fig. 2, the cell *OCV* decreased from 1.024 V at 20 vol % AH to 0.978 V at 60 vol % AH. From Fig. 2, it can be also seen that the cell voltage varies linearly with the current density up to a value that depends on the AH, indicating that the cell is reversible.

Figures 3a–1 and 3b–1 show impedance results for cell–1 (having Ni-SDC hydrogen electrode) with different steam concentrations (20, 40, and 60 vol % AH, respectively) at 850°C using a two–electrode method under both OCV and 60 mA cm^{-2} electrolysis current conditions, respectively. It can be seen that cell resistances increase with the increase in steam concentration in the feeding gas, from 1.585 $\Omega\cdot cm^2$ with 20 vol % AH to 1.712 $\Omega\cdot cm^2$ with 60 vol % AH under OCV, and from 1.35 $\Omega\cdot cm^2$ with 20 vol % AH to 1.582 $\Omega\cdot cm^2$ with 60 vol % AH under 60 $mA\cdot cm^{-2}$ electrolysis current. Moreover, the impedance spectra were typically characterized by two semicircles in the frequency domain studied, similar to the data reported by Hauch and co–workers,[26,27] indicating that the SOEC was controlled by at least two electrode processes during the high temperature steam electrolysis. Characteristic frequencies were labeled in the impedance spectra. The impedance spectra recorded under OCV consist of two arcs with summit frequencies of 1.99 kHz and 19.95 Hz, respectively. The arc with a summit frequency of 1.99 kHz can be assigned to gas–solid (adsorption, dissociation, desorption) or solid–solid reaction (surface diffusion and oxygen transfer to/from the electrolyte) which typically has summit frequency in the range of 100 to 10 kHz. The arc with a summit frequency of 19.95 Hz can be assigned to gas conversion and/or diffusion with characteristic frequency in the range of 10–100 Hz.[28] Figures 3a–2 and 3b–2 are the impedance results of the hydrogen electrode with different humidity under OCV and 60 $mA\cdot cm^{-2}$ electrolysis current density conditions tested by a three–electrode method. Figures 3a–3 and 3b–3 are the impedance results of the oxygen electrode with the same testing conditions. Impedance of the hydrogen electrode increased with the increase in steam concentrations, while that of the oxygen electrode was very slightly influenced by the increase in steam concentrations. Further, compared

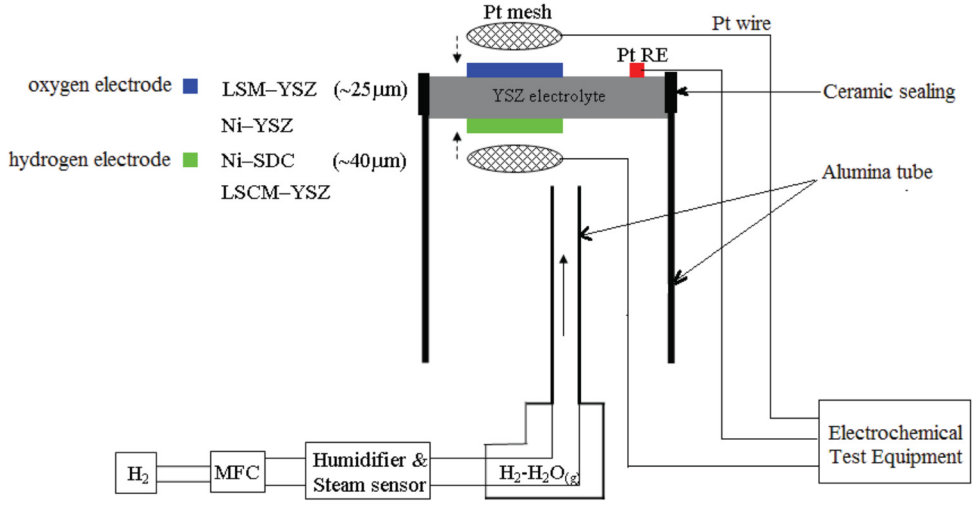

Figure 1. (Color online) Schematic representation of the experimental setup employed for high temperature steam electrolysis measurements.

Table II. Open circuit voltages (OCVs) of three types of cells at different steam content at 850°C.

	Cell–1 (V)	Cell–2 (V)	Cell–3 (V)
20 AH	1.024	1.014	1.031
40 AH	0.994	0.988	1.023
60 AH	0.978	0.979	0.984
80 AH	—	0.953	0.968

with the characteristic summit frequencies of the cell shown in Figs. 3a–1 and 3b–1, it can be concluded that the high–frequency arc (1.99 kHz) of the cell is associated with the hydrogen electrode, while the low–frequency arc (19.95 Hz) is associated with the oxygen electrode.

Taking the cell–1 impedance spectra data with different steam concentration measured under OCV as an example, the impedance data were fitted and analyzed using Zview software. The equivalent circuit for fitting the impedance spectra is given in Fig. 4. Fitting curves are also plotted in Fig. 3a–1 and the fitting results are shown in Table III. The series resistance, R_s, corresponds to the overall ohmic resistance from the electrolyte, electrodes and the lead wires; *CPE* is the constant–phase element, while (R_1, CPE_1) and (R_2, CPE_2) correspond to the high and low frequency arcs, respectively. The total interfacial polarization resistance (R_p) of the cell is the sum of R_1 and R_2. As shown in Table III for cell–1 fitting data, in the steam concentration range studied, R_1 increased with the increase in steam concentrations, while R_2 was relatively constant. The fitting values of R_1 and R_2 were consistent to those shown in Fig. 3a–2 for the hydrogen electrode and in Fig. 3a–3 for the oxygen electrode, respectively. Analysis of the impedance results indicate that the resistance in the high frequency range primarily comes from the hydrogen electrode while the resistance in the low frequency range comes from the oxygen electrode. From the fitting results, it can be also observed that R_1 is always larger than R_2, implying that the cell resistance is dominated by the hydrogen electrode process. This result is similar to some modeling study.[20] Further, the percentage changes in ohmic and polarization resistances from the baseline 20 AH are given in Table III. It can be seen that steam concentration mainly affects the cell polarization resistance.

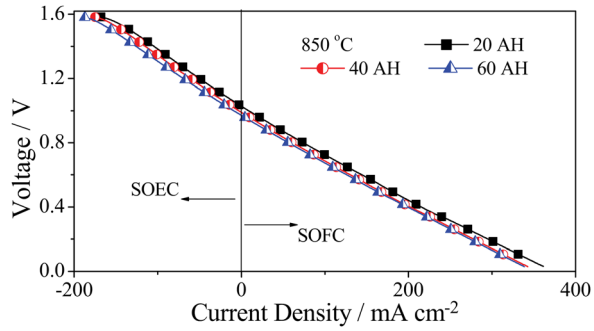

Figure 2. (Color online) Voltage–current density curves of cell–1 with different steam content operated under SOEC and SOFC mode at 850°C.

The overpotentials of the hydrogen electrode and the oxygen electrode in different steam concentration testing conditions for

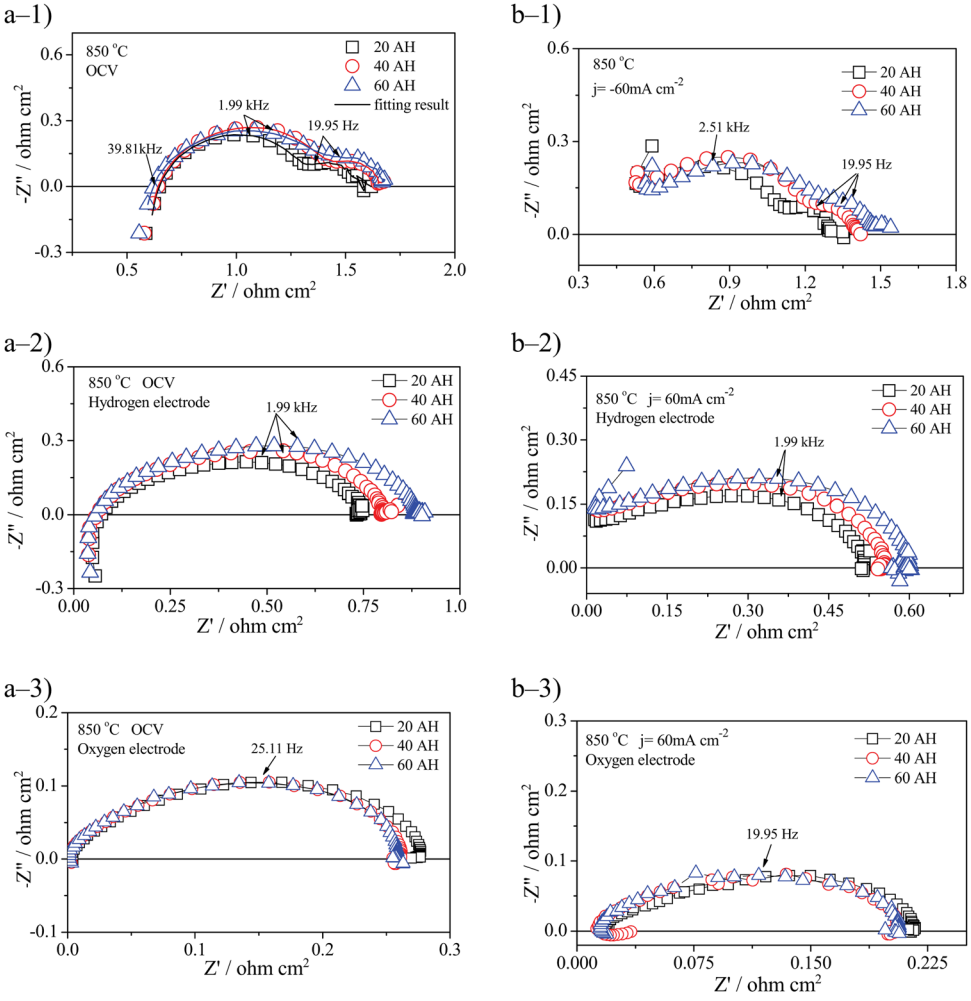

Figure 3. (Color online) Electrochemical impedance spectra of cell–1 with different steam content at 850°C under OCV and electrolysis process. Figures 3(a–1) and 3(b–1) are the cell impedance spectra measured by the two–electrode method; Figs 3(a–2) and 3(b–2) show the impedance spectra of the hydrogen electrode measured by the three–electrode method; Figs. 3(a–3) and 3(b–3) are the impedance spectra of the oxygen electrode measured by the three–electrode method.

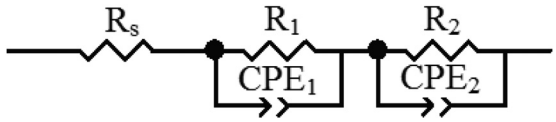

Figure 4. Equivalent circuit used to fit the impedance data of these three types of SOECs under OCV conditions.

cell–1 were evaluated via a three–electrode method and presented in Fig. 5. It should be noted that, according to the cell configuration shown in Fig. 1, the measured overpotential of the hydrogen electrode comprises the ohmic voltage drop (*IR* drop) across the electrolyte. The value of *IR* drop can be estimated, where *I* is the cell polarization current and *R* is the resistance of the YSZ electrolyte which can be calculated from the following equation:[29]

$$R = \frac{1}{\sigma}\frac{l}{(1/4)\pi d^2} \quad (2)$$

where σ is the conductivity of the YSZ electrolyte at a given temperature, *l* is the thickness of the YSZ electrolyte membrane (0.03 cm in this study), and *d* is the diameter of the YSZ electrolyte (2.00 cm in this study). Since *IR* drop is the same under a given current, the calculated value of *IR* drop is not subtracted from the measured overpotential of the hydrogen electrode as shown in Fig. 5. It can be seen that the overpotential in the oxygen electrode is insensitive to the steam concentration, indicating that steam concentration does not affect the migration of oxygen ions from the YSZ electrolyte to the LSM–YSZ/LSM oxygen electrode in the electrolysis process. On the contrary, the overpotential of the hydrogen electrode increases with the increase in the steam concentrations, consistent to the impedance spectra results.

The impedance results of cell–2 (having Ni-YSZ hydrogen electrode) with the same testing conditions were measured and displayed in Figs. 6a–1 and 6b–1, and the contributions of the hydrogen electrode and oxygen electrode tested by a three–electrode method under OCV and electrolysis current of 60 mA cm^{-2} were shown in Fig. 6. Similar to cell–1, increase in cell resistance with the increase in steam concentration has been observed, and the impedance spectra were also typically characterized by two semicircles. According to the characteristic summit frequencies labeled in these figures, the high–frequency arc (~15.84 kHz) of the cell is associated with the hydrogen electrode, while the low–frequency arc (~7.94 Hz) is associated with the oxygen electrode. Based on the analysis of the impedance spectra (shown in Table III), the cell reaction is also dominated by the hydrogen electrode process for cell–2.

Evaluation of cells with LSCM–based hydrogen electrode.— As an electrochemically active and redox stable SOFC anode material, $La_{0.75}Sr_{0.25}Cr_{0.5}Mn_{0.5}O_3$ (LSCM) has also been reported as an effective hydrogen electrode material in high temperature electrolysis process.[24,30,31] Figures 7a–1 and 7b–1 show impedance spectra of cell–3 (having LSCM-YSZ hydrogen electrode) with different steam concentration tested at 850°C by a two–electrode method under both OCV and 60 mA cm^{-2} electrolysis current density conditions, respectively. It can be seen that cell resistance increased with the increase in steam concentration. It is well known that the electrode polarization typically decreases when current is applied to the cell compared with that under OCV condition, and the cell polarization resistance, especially the activation polarization resistance decreases with the increase in cell current density. Compared with the resistance under OCV (shown in Fig. 7a–1), the total cell resistance (R_t) and the cell polarization resistance (R_p) decreased under the electrolysis process (shown in Fig. 7b–1). The total resistance decreased from 2.15 Ω cm^2 under OCV to 1.79 Ω cm^2 under electrolysis condition with 20 vol % AH, and 2.43 Ω cm^2 under OCV to 1.94 Ω cm^2 under electrolysis condition with 80 vol % AH. The impedance contributions of the hydrogen electrode and the oxygen electrode were further separated through the Pt reference electrode. Figures 7a–2 and 7b–2 present the contributions of the hydrogen electrode under OCV and the electrolysis process, while Figs. 7a–3 and 7b–3 are those of the oxygen electrode in both conditions. It can be seen that steam concentration in the hydrogen electrode affects the contribution of the hydrogen electrode, but has very little effect on the oxygen electrode. The impedance data under OCV were fitted using the same equivalent circuit as displayed in Fig. 4, and the fitting results were also given in Table III. The impedance spectra of cell–3 can be divided into two parts, but they are different from those of cell–1 and cell–2 (the Ni–based SOECs). The impedance arc associated with the hydrogen electrode overlaps with that associated with the oxygen electrode, and the impedance values from both electrodes are similar in magnitude.

Figure 8 shows effect of the steam concentration on overpotentials of both the hydrogen and oxygen electrode for cell–3. Since *IR* drop is the same under a given current, the calculated value of *IR* drop is not subtracted from the measured overpotential of the hydrogen electrode in the figure. From Fig. 8, it can be observed that the overpotential of the hydrogen electrode increased with the increase in steam concentrations, while the overpotenital of the oxygen electrode seems to be not affected by the steam concentrations.

In the high temperature steam electrolysis process, the overall electrode reactions can be represented as Step 1–Step 8:

$$\text{Step 1: } H_2O_{(g)} \rightarrow H_2O_{ad} \quad (3)$$

Table III. Fitting results of the electrochemical impedance spectra under OCV for three types of cells.

	R_s (Ω cm^2)	R_1 (Ω cm^2)	CPE_1 (Ω cm^2 s^{-n})	R_2 (Ω cm^2)	CPE_2 (Ω cm^2 s^{-n})	R_1+R_2 (Ω cm^2)	ΔR_s (%)	$\Delta(R_1+R_2)$ (%)
Cell–1								
20 AH	0.665	0.627	0.410	0.293	0.378	0.920	0	0
40 AH	0.653	0.727	0.405	0.285	0.406	1.003	− 1.80	9.02
60 AH	0.652	0.761	0.382	0.299	0.387	1.060	− 1.95	15.22
Cell–2								
20 AH	0.567	1.927	0.131	0.442	0.223	2.369	0	0
40 AH	0.539	2.194	0.128	0.379	0.231	2.573	− 4.94	8.61
60 AH	0.543	2.300	0.124	0.336	0.238	2.636	− 4.23	11.27
80 AH	0.483	2.461	0.118	0.275	0.247	2.736	− 14.81	15.49
Cell–3								
20 AH	0.575	0.712	0.296	0.863	0.352	1.575	0	0
40 AH	0.584	0.841	0.386	0.795	0.291	1.636	1.56	3.87
60 AH	0.568	0.874	0.317	0.871	0.355	1.745	− 1.22	10.79
80 AH	0.649	0.870	0.302	0.797	0.348	1.667	12.86	5.84

Note: ΔR_s and $\Delta(R_1+R_2)$ are percentage change in ohmic and electrode polarization resistance from the baseline 20 AH, respectively.

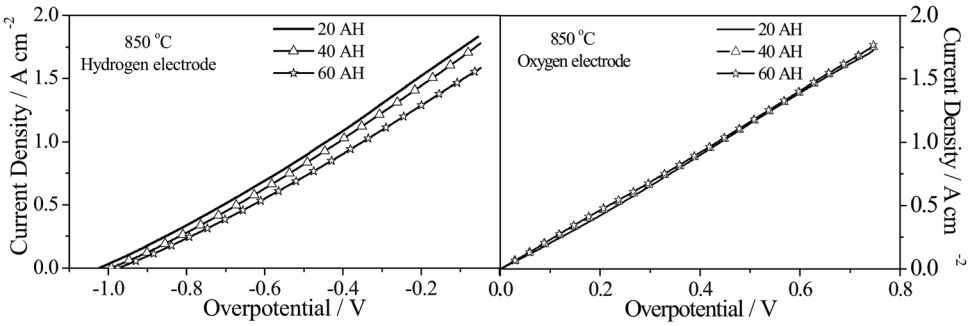

Figure 5. Overpotential of the hydrogen and oxygen electrode for cell–1 under different steam concentration.

$$\text{Step 2: } H_2O_{ad} \rightarrow OH^-_{ad} + H^+_{ad} \quad (4)$$

$$\text{Step 3: } OH^-_{ad} \rightarrow O^{2-}_{ad} + H^+_{ad} \quad (5)$$

$$\text{Step 4: } O^{2-}_{ad} - e \rightarrow O^-_{ad} \quad (6)$$

$$\text{Step 5: } O^-_{ad} - e \rightarrow O_{ad} \quad (7)$$

$$\text{Step 6: } 2O_{ad} \rightarrow O_2(ad) \quad (8)$$

$$\text{Step 7: } H^+_{ad} \rightarrow H^+_{TPB} \quad (9)$$

$$\text{Step 8: } 2H^+_{TPB} + 2e \rightarrow H_2 \quad (10)$$

where Step 1–Step 3 describe the surface dissociative adsorption of steam to O^{2-}_{ad} and H^+_{ad}; Step 4–Step 6 illustrate the formation and desorption of O_2 along with the charge transfer process; Step 7 and Step 8 refer to H^+_{ad} migration to triple phase boundaries (TPBs) and H_2 generation. He and co–workers[32] have analyzed the impedance spectra of reversible SOFCs with proton conducting electrolyte and concluded that the migration of H^+_{ad} to TPBs of the hydrogen electrode corresponds to the high frequency arc in the electrochemical impedance spectra, and the surface diffusion of O^-_{ad} corresponds to the low frequency arc. Since O^{2-} and O^- can readily donate electrons on the surface of LSM and consequently there is no need for them to be transported to the TPBs. Consequently, the surface diffusion of O^-_{ad} is not an elementary step in the electrolysis process. This is consistent with the impedance spectra data.

Meng and co-workers[20] have found that the hydrogen electrode is vulnerable to high concentration overpotential and limiting current density in the SOEC mode through a modeling study. The experimental results of these three types of cells indicate that steam concentration in the feeding gas affects the cell resistance, especially from the contribution of the hydrogen electrode. With the increase in steam content, the change in cell resistance is mainly

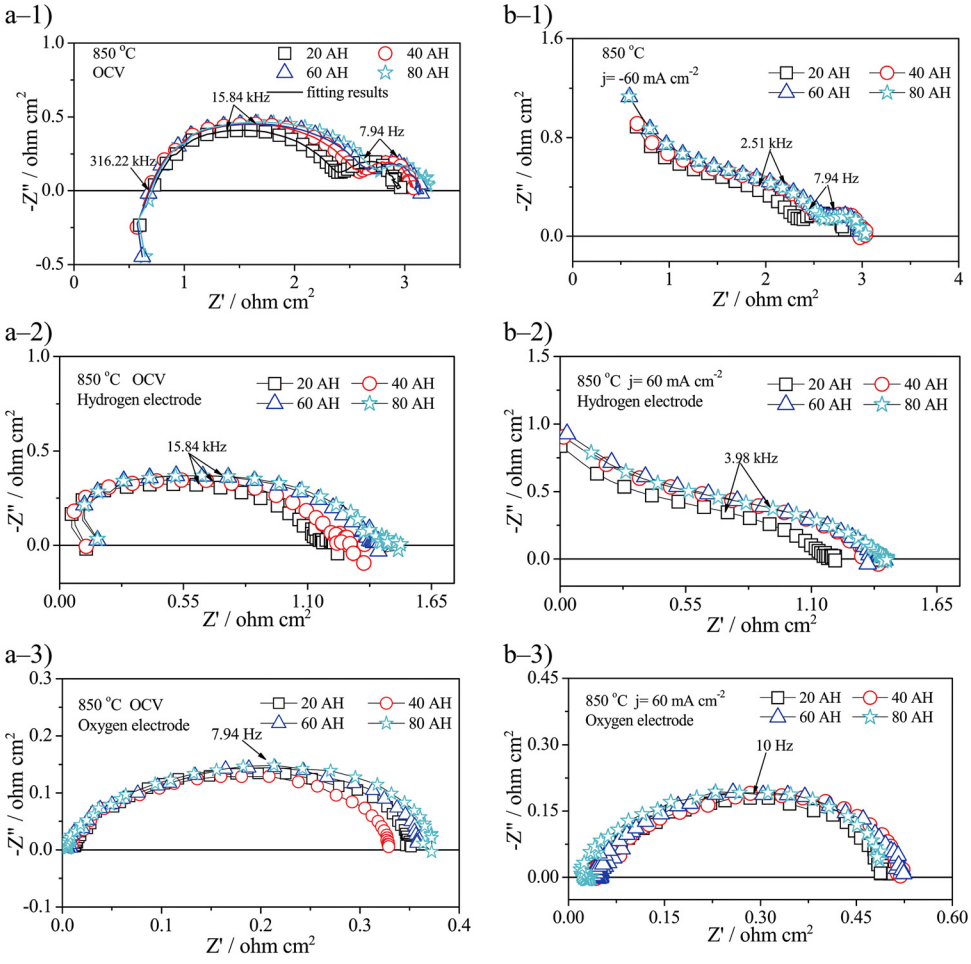

Figure 6. (Color online) Electrochemical impedance spectra of cell–2 with different steam content at 850°C under OCV and electrolysis process. Figures 6(a–1) and 6(b–1) are the cell impedance spectra measured by the two–electrode method; Figs. 6(a–2) and 6(b–2) show the impedance spectra of the hydrogen electrode measured by the three–electrode method; Figs. 6(a–3) and 6(b–3) are the impedance spectra of the oxygen electrode measured by the three–electrode method.

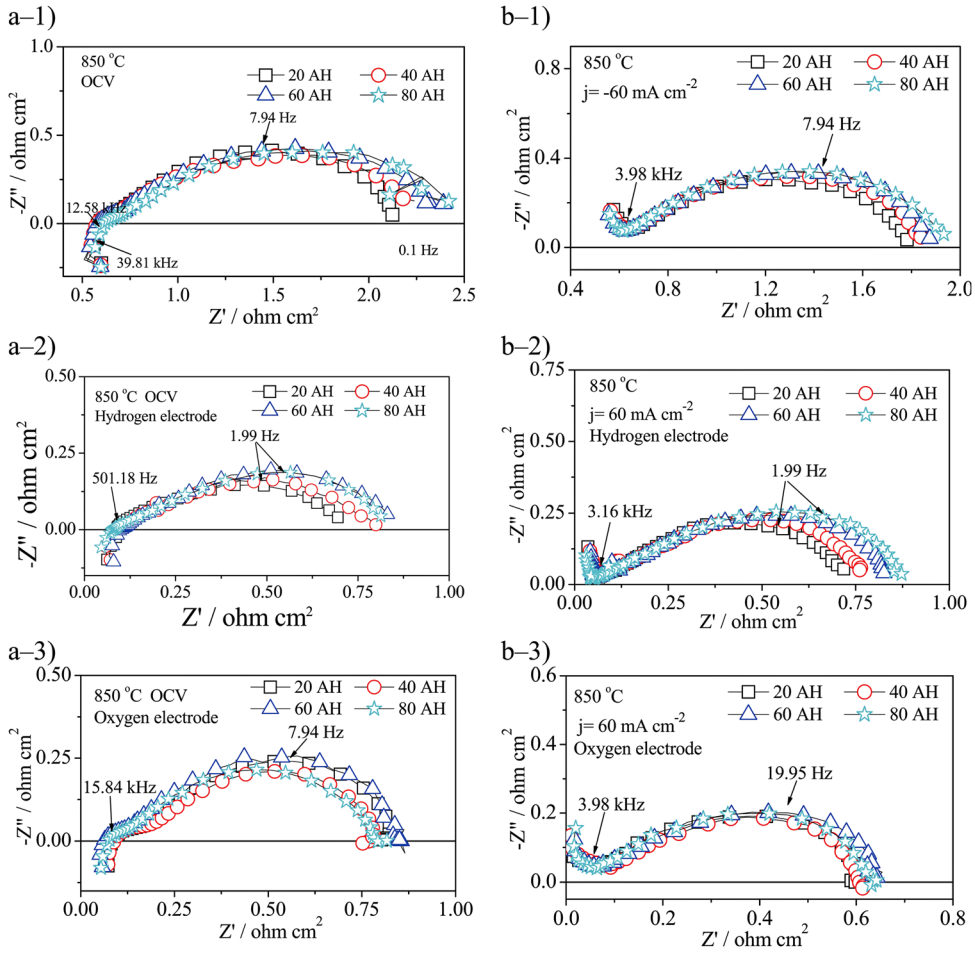

Figure 7. (Color online) Electrochemical impedance spectra of cell–3 with different steam content at 850°C under OCV and electrolysis process. Figures 7(a–1) and 7(b–1) are the cell impedance spectra measured by the two–electrode method; Figs. 7(a–2) and 7(b–2) show the impedance spectra of the hydrogen electrode measured by the three–electrode method; Figs. 7(a–3) and 7(b–3) are the impedance spectra of the oxygen electrode measured by the three–electrode method.

due to the increased resistance of the hydrogen electrode. Various explanations have been proposed to account for this phenomenon. Williford and co–workers[33,34] considered gas diffusion as one of the dominating reasons to affect the performance of the SOFC anode. In this study, gas diffusion seems also to be one of the dominating reasons to affect the performance of the hydrogen electrode in the electrolysis process. Gas transport in porous electrode is primarily through diffusion. Zhan[35] studied the gas diffusivity in different gas mixtures in the high temperature electrolysis process and found that the gas diffusivity of heavier steam molecules was much smaller than that of lighter hydrogen molecules. For example, the diffusion coefficient of steam is 3.80 cm^2/s, while that of hydrogen is 5.74 cm^2/s in hydrogen-steam mixture at 800°C.[35] It has been reported that higher polarization losses for the hydrogen electrode are predicted during electrolysis process, mainly because of the difference in H_2 and H_2O diffusions.[36] For Ni–based SOEC, two other possible reasons can be used to interpret the phenomenon. It is well known that coarsening of Ni particles is accelerated under high steam content at elevated temperatures.[37] Consequently, change in the hydrogen electrode microstructure such as Ni particle agglomeration will lead to a decrease in the length of TPBs where the electrochemical reaction takes place.[38] The functional layer of the hydrogen electrode utilized in the present study is ~40 μm thick. Thinner electrodes (< 10 μm) and smaller particles have been reported to be more susceptible to rapid degradation at high steam partial pressure than the thick electrode and coarse electrode structure.[38] It is also well known that nickel is not a redox stable material. Localized surface oxidation of Ni under high steam environment, forming a less active layer, has been proposed as another possible cause of performance degradation of the hydrogen electrode under the electrolysis process.[10] It has been reported that the polarization of the Ni-based hydrogen electrode increases with the increase in operating oxygen partial pressure due to surface oxidation of metal,[39] which indicates that the use of a precious metal may be preferable under high steam conditions. In contrast to the Ni–YSZ electrode, much enhanced electrochemical activity for operating in electrolysis mode

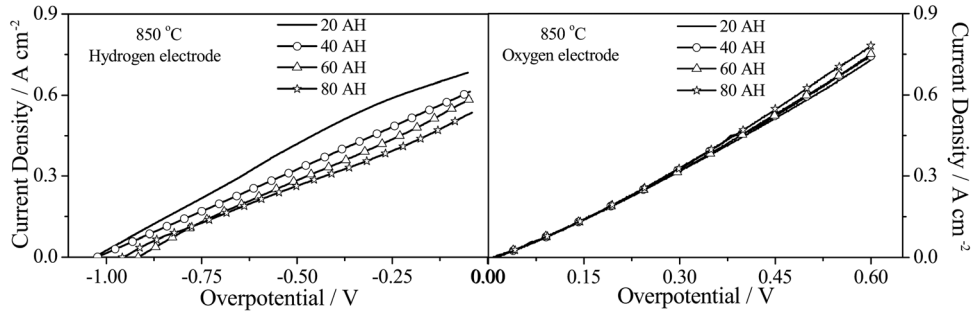

Figure 8. Overpotential of the hydrogen and oxygen electrode for cell–3 under different steam concentration.

was achieved with the Ni–SDC electrode, suggesting that inclusion of SDC in the composite hydrogen electrode is beneficial to the electrolysis process. It is likely that the oxygen storage capacity of SDC helps to suppress the oxidation of the Ni surface and leads to higher performance in the electrolysis process.[36] LSCM–YSZ hydrogen electrode also shows better performance than that of the Ni–YSZ hydrogen electrode in the electrolysis mode. Better redox stability of LSCM and mixed oxide ionic and electronic conductivity are expected to be the main reasons for the enhanced electrochemical performance of the LSCM-YSZ hydrogen electrode.

Conclusions

From the electrochemical characterization of the three types of cells for high temperature steam electrolysis, the following conclusions can be made:

1. Steam content of the feeding gas affects the cell performance in SOECs and electrolysis reactions become difficult with the increase in steam concentration.
2. Steam concentration affects the contribution of the hydrogen electrode in the electrolysis process, while it has little effect on the oxygen electrode.
3. Contribution from the hydrogen electrode is dominant in the electrolysis reactions for Ni–based SOECs, but this contribution decreases for LSCM–based SOECs.

Acknowledgment

Financial support from NASA EPSCoR (Award No. NNX10AN33A) and the Department of Energy (Award No. DE-10EE0003222) is gratefully acknowledged.

References

1. M. Ball and M. Wietschel, *Int. J. Hydrogen Energy*, **34**, 615 (2009).
2. N. Laosiripojana and S. Assabumrungrat, *Appl. Catal. B*, **82**, 103 (2008).
3. S. H. Yoon, J. M. Bae, S. Y. Kim, and Y. S. Yoo, *J. Power Sources*, **192**, 360 (2009).
4. N. Laosiripojana and S. Assabumrungrat, *J. Power Sources*, **158**, 1348 (2006).
5. S. H. Jensen, P. H. Larsen, and M. Mogensen, *Int. J. Hydrogen Energy*, **32**, 3253 (2007).
6. A. Hauch, S. H. Jensen, S. Ramousse, and M. Mogensen, *J. Electrochem. Soc.*, **153**, A1741 (2006).
7. J. E. O'Brien, C. M. Stoots, J. S. Herring, P. A. Lessing, J. J. Hartvigsen, and S. Elangovan, *J. Fuel Cell Sci. Technol.*, **2**, 156 (2005).
8. C. M. Stoots, J. E. O'Brien, K. G. Condie, and J. J. Hartvigsen, *Int. J. Hydrogen Energy*, **35**, 4861 (2010).
9. Z. W. Wang, M. Mori, and T. Araki, *Int. J. Hydrogen Energy*, **35**, 4451 (2010).
10. K. Eguchi, T. Hatagishi, and H. Arai, *Solid State Ionics*, **86–88**, 1245 (1996).
11. J. S. Herring, J. E. O'Brien, C. M. Stoots, G. L. Hawkes, J. J. Hartvigsen, and M. Shahnam, *Int. J. Hydrogen Energy*, **32**, 440 (2007).
12. Y. Huang, J. M. Vohs, and R. J. Gorte, *J. Electrochem. Soc.*, **152**, A1347 (2005).
13. S. P. Jiang and J. G. Love, *Solid State Ionics*, **138**, 183 (2001).
14. M. J. Jorgensen, S. Primdahl, and M. Mogensen, *Electrochim. Acta*, **44**, 4195 (1999).
15. K. Yasumoto, N. Mori, J. Mizusaki, H. Tagawa, and M. Dokiya, *J. Electrochem. Soc.*, **148**, A105 (2001).
16. A. Mitterdorfer and L. J. Gauckler, *Solid State Ionics*, **111**, 185 (1998).
17. T. Horita, K. Yamaji, H. Negishi, N. Sakai, H. Yokokawa, and T. Kato, *Solid State Ionics*, **137**, 897 (2000).
18. T. Jacobsen, B. Zachau–Christiansen, L. Bay, and M. J. Jorgensen, *Electrochim. Acta*, **46**, 1019 (2001).
19. W. S. Wang, Y. Y. Huang, S. Jung, J. M. Vohs, and R. J. Gorte, *J. Electrochem. Soc.*, **153**, A2066 (2006).
20. N. Meng, K. H. Michael, and Y. C. L. Dennis, *J. Power Sources*, **163**, 460 (2006).
21. B. Huang, S. R. Wang, R. Z. Liu, X. F. Ye, H. W. Nie, and X. F. Sun, *J. Power Sources*, **167**, 39 (2007).
22. C. H. Yang, C. Jin, A. Coffin, and F. L. Chen, *Int. J. Hydrogen Energy*, **35**, 5187 (2010).
23. C. H. Yang, C. Jin, and F. L. Chen, *Electrochim. Acta*, **56**, 80 (2010).
24. C. Jin, C. H. Yang, F. Zhao, D. A. Cui, and F. L. Chen, *Int. J. Hydrogen Energy*, **36**, 3340 (2011).
25. J. Rutman and I. Riess, *Electrochim. Acta*, **52**, 6073 (2007).
26. A. Hauch, S. H. Jensen, S. Ramousse, and M. Mogensen, *J. Electrochem. Soc.*, **153**, A1741 (2006).
27. A. Hauch and M. Mogensen, *Solid State Ionics*, **181**, 745 (2010).
28. A. Brisse, J. Schefold, and M. Zahid, *Int. J. Hydrogen Energy*, **33**, 5375 (2008).
29. H. M. Xiao, T. L. Reitz, and M. A. Rottmayer, *J. Power Sources*, **183**, 49 (2008).
30. X. D. Yang and J. T. S. Irvine, *J. Mater. Chem.*, **18**, 2349 (2008).
31. F. Bidrawn, G. Kim, G. Corre, J. T. S. Irvine, J. M. Vohs, and R. J. Gorte, *Electrochem. Solid–State Lett.*, **11**, B167 (2008).
32. F. He, D. Song, R. R. Peng, G. Y. Meng, and S. F. Yang, *J. Power Sources*, **195**, 3359 (2010).
33. R. E. Williford, L. A. Chick, G. D. Maupin, S. P. Simner, and J. W. Stevenson, *J. Electrochem. Soc.*, **150**, A1067 (2003).
34. Y. Jiang and A. V. Virkar, *J. Electrochem. Soc.*, **150**, A942 (2003).
35. Z. L. Zhan, W. Kobsiriphat, J. R. Wilson, M. Pillai, I. Kim, and S. A. Barnett, *Energy Fuels*, **23**, 3089 (2009).
36. P. K. Lohsoontorn and J. Bae, *J. Power Sources*, **196**, 7161 (2011).
37. J. Sehested, *Catal. Today*, **111**, 103 (2006).
38. O. A. Marina, L. R. Pederson, M. C. Williams, G. W. Coffey, K. D. Meinhardt, C. D. Nguyen, and E. C. Thomsen, *J. Electrochem. Soc.*, **154**, B452 (2007).
39. K. Eguchi, Y. Kunisa, K. Adachi, M. Kayano, K. Skizawad, and H. Arai, *Chem. Lett.*, **24**, 963 (1995).